ELSEVIER

Coordination Chemistry Reviews 226 (2002) 235–249

COORDINATION CHEMISTRY REVIEWS

www.elsevier.com/locate/ccr

Spin-mediated superconductivity in cuprates, organic conductors and π–d conjugated systems

Kizashi Yamaguchi [a,*], Yasutaka Kitagawa [a], Taku Onishi [a], Hiroshi Isobe [a], Takashi Kawakami [a], Hidemi Nagao [b], Satoshi Takamizawa [c]

[a] *Department of Chemistry, Graduate School of Science, Osaka University, Toyonaka, Osaka 560-0043, Japan*
[b] *Department of Computational Science, Faculty of Science, Kanazawa University, Kakuma, Kanazawa 920-1192, Japan*
[c] *Department of Chemistry, Faculty of Science, Yokohama City University, Yokohama, Kanagawa 236-0027, Japan*

Received 9 May 2001; accepted 21 September 2001

Contents

Abstract

Previous theoretical models of organometallic magnetic conductors and superconductors are examined on the basis of ab initio Hamiltonians and Hubbard models for clusters of p–d and π–d systems in relation to the recently developed π–d systems such as $(BEDT\text{-}TTF)_2Y$ and $(BETS)_2Y$ ($Y = Cu(NCS)_2$, $Cu[N(CN)_2]X$, $Fe(III)X_4$ (X = halogens, etc.)). The Fe(III) complexes have been used as spin sources in these systems. The phase diagrams observed for the species are similar to those of cuprate and heavy fermion superconductors because of the existence of a magnetic phase near superconducting phase. In order to elucidate the characteristic electronic structures of these species, effective exchange integrals (J_{ab}) for magnetic clusters are calculated by ab initio density functional (DFT) methods. From the computational results, several model Hamiltonians such as t–J, Kondo and RKKY models are examined for a theoretical understanding of the experimental phase diagrams. Theoretical possibilities of

* Corresponding author. Tel.: +81-6-6850-5405; fax: +81-6-6850-5550.
E-mail address: yama@chem.sci.osaka-u.ac.jp (K. Yamaguchi).

PII: S0010-8545(01)00440-4

magnetic conductors and spin-mediated superconductors are discussed on the basis of these models in the intermediate region for metal-insulator transitions. The importance of electron correlation and lattice dimensionality is emphasized in relation to high-T_c superconductivity.

Keywords: Spin mediated superconductivity; π–d Conjugated system; DFT calculation; Effective exchange integrals; BEDT-TTF; Copper oxide

1. Introduction

During the past decade, molecular magnets, molecular conductors, and their hybrid systems in intermediate or strong electron correlation (EC) regimes have attracted much interest in relation to the high-T_c superconductivity in copper oxides [1]. Much experimental and theoretical effort has been made for the elucidation of a possible interplay between the p- and d-electrons of transition-metal oxides in such a regime [2–4]. Now it is well established that copper oxides are antiferromagnets before doping, while the species after doping exhibit the high-T_c superconductivity. In a previous paper [5], we have examined several model Hamiltonians for copper oxides to elucidate the mechanism of the high-T_c superconductivity; (1) t–J model, (2) spin-fluctuation model, (3) spin- and charge-fluctuation model, which is referred to as an EC model [5], and (4) charge-fluctuation or CT model. Now, the models (1)–(3) are compatible with the accumulated experimental results for copper oxides [4]. Previously [5], we have also investigated possible organic, organometallic and inorganic analogs to copper oxides on the basis of these models (1)–(4), which permit the nonconventional BCS mechanisms such as *d*-wave superconductivity.

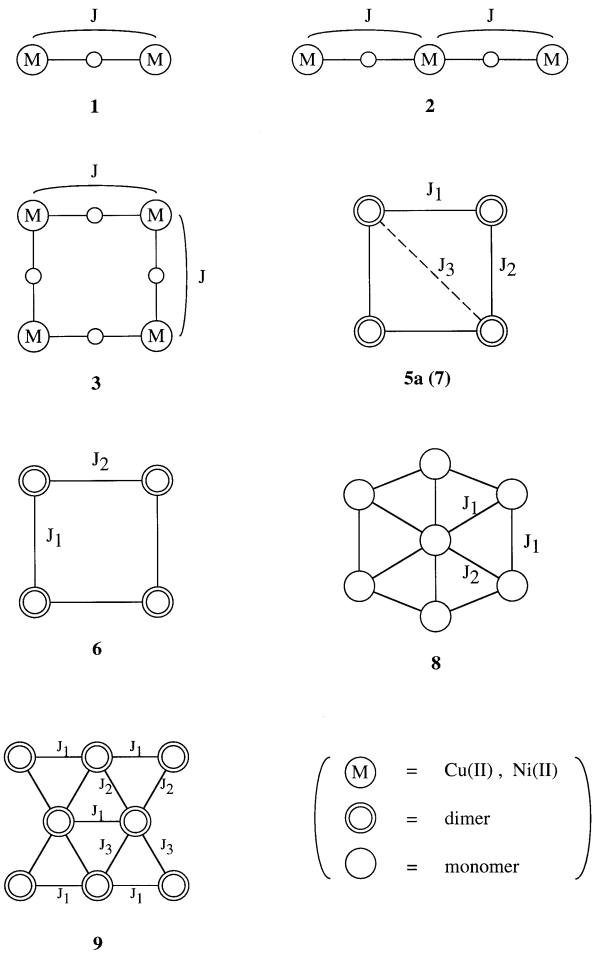

Fig. 1. The binuclear clusters (**1**–**3**) extracted from the K_2NiF_4-type solid and dimer (or monomer) models of organic conductors (**4**–**9**) with triangular and square planar sheets.

In the present paper, we first review the ab initio calculations of effective exchange integrals (J_{ab}) for copper oxides and related species, and the t–J model for high-T_c copper oxides. We also examine recently developed π–d conjugated systems such as $(BEDT\text{-}TTF)_2Y$ and $(BETS)_2Y$ ($Y = Cu(NCS)_2$, $Cu[N(CN)_2]X$, $Fe(III)X_4$ (X = halogens, etc.)). The Fe(III) complexes have been used as spin sources in these systems. The phase diagrams observed for the species are similar to those of cuprate and heavy fermion superconductors because of the existence of a magnetic phase near the superconducting phase. Our J model is successfully applied to these π–d systems to obtain a unified picture of the magnetism and superconductivity in strongly EC systems. Finally, implications of the calculated results are discussed in relation to molecular design of new extended coordination compounds, which are constructed of transition metals and π-electron networks in two and fractal dimensions [6–8].

2. Ab initio computation of effective exchange integrals

2.1. Effective exchange integrals for transition metal oxides

As is well known [4,9], conventional density functional theory (DFT) such as BLYP overestimate metallic character, and copper oxides become a metal instead of an antiferromagnetic (AF) insulator under the DFT approximation. Previously [9], we have shown that hybrid DFT(HDFT) methods can be used for strongly correlated electron systems such as manganese oxides. Therefore, copper oxides and nickel oxides are appropriate examples for explanation of the utility of HDFT methods. These metal oxides form the 1D chain and 2D layered perovskite-type structures. First of all, let us consider cluster models (**1**) in Fig. 1 in order to explain the ab initio computational schemes of effective ex-

change integrals (J_{ab}) in the Heisenberg model [9]. The linear cluster model (**2**) is investigated as the simplest model for 1D Sr_2CuO_3 and Sr_2CuO_2 crystals [10–14]. It is known that the MO_2 sheets are mainly responsible for magnetic properties for K_2NiF_4-type transition metal oxides [15,16] such as La_2CuO_4 and $YBa_2Cu_3O_6$. We therefore constructed the square planar M_4O_4 (model **3**) as the simplest model for our theoretical investigation.

The J_{ab} values are given by using spin-projected and unprojected schemes as [9]

$$J_{ab}^{(1)} = \frac{^{LS}E(X) - {}^{HS}E(X)}{^{HS}\langle S^2\rangle - {}^{LS}\langle S^2\rangle} \quad (1)$$

$$J_{ab}^{(2)} = \frac{^{LS}E(X) - {}^{HS}E(X)}{4(N-1)S_aS_b} \quad (2)$$

where $^{Y}E(X)$ and $^{Y}\langle S^2\rangle$ denote, respectively, the total energy and total spin angular momentum for state Y by the method X. In order to explain ab initio computational methods in Eqs. (1) and (2), we have calculated effective exchange integrals (J_{ab}) for **1**–**3** by the UHF and Hybrid-DFT methods [17,18]. Table 1 summarizes the J_{ab} for copper and nickel oxides (**1**–**3**). All the J_{ab} values are negative, showing the AF interaction in accord with the experiments [10–14]. From Table 1, the spin-projected $|J_{ab}^{(1)}|$ value for CuOCu (**1a**) by each BS method is a little smaller than the unprojected $|J_{ab}^{(2)}|$ value because of the non-negligible orbital overlap between the magnetic orbitals. The spin-projected $|J_{ab}^{(1)}|$ value for the linear cluster CuOCuOCu (**2a**) by each BS method is close to the unprojected $|J_{ab}^{(2)}|$ value, indicating that the orbital overlap effect is rather small, even in the case of the half-and-half (HH)-type DFT method. The $|J_{ab}^{(1)}|$ value for **2a** by UHF is about one tenth of HH-type DFT method. Experimentally, the $|J_{ab}|$ values are -904 cm^{-1} for Sr_2CuO_3 [12] obtained by the magnetic susceptibility measurement, and -765 cm^{-1} for Sr_2CuO_2 by the same method [13], while a value of -1049 cm^{-1} is found for Sr_2CuO_3 by the midinfrared optical absorption method [14]. From these data, the J_{ab} value for the 1D chain is in the range; -765 to -1049 cm^{-1}. The present HH-type DFT cluster model calculations reproduced well the experimental results [12,13], in sharp contrast with conventional DFT methods.

The $|J_{ab}^{(1)}|$ value for the tetranuclear ring Cu_4O_4 (**3a**) is significantly smaller than the $|J_{ab}^{(2)}|$ value by each BS method. This implies that the orbital overlap effect is not negligible because of the electron delocalization (see also below). The $|J_{ab}^{(1)}|$ value for **3a** by UHF is about 1/5–1/7 of the HH-type DFT methods. Experimentally [10–14], the J_{ab} values are -484, -488, -536 and -625 cm^{-1} for $YBa_2Cu_3O_{6.15}$, Pr_2CuO_4, La_2CuO_4 and Nd_2CuO_4, respectively. Then, we may consider that the J_{ab} value is in the range; -484 to -625 cm^{-1}, though the Cu–O–Cu distances are different among the four oxides, and the correlation between the observed J_{ab} value and Cu–O length is complex [10]. From Table 1, we conclude that the HH-type DFT calculations for **3a** can reproduce the experimental J_{ab} values for the copper oxides, though computation of larger clusters are desirable for refinement of the calculated results for **3a**.

In order to confirm the calculated results for the copper oxides, we have performed the same computation on the nickel oxides clusters **1b**–**3b**. Similar tendencies are also recognized for the computational results for NiONi (**1b**) and NiONiONi (**2b**). The $|J_{ab}^{(1)}|$ value for Ni_4O_4 (**3b**) is smaller than the $|J_{ab}^{(2)}|$ value, showing a non-negligible orbital overlap effect which entails the necessity of the approximate spin projection (AP). Indeed, the $|J_{ab}^{(1)}|$ values for **3b** by the HH-type DFT methods with the AP procedure are close to the experimental value [15,16]. The $|J_{ab}^{(1)}|$ values of **3b** for the 2D sheet model are smaller than those of **2b** for the 1D chain model. The same tendency is also recognized for the copper oxides (**3a** and **2a**). This is consistent with experimental observation [10–14]. In conclusion,

Table 1
Effective exchange integrals (J_{ab}) [a] calculated for transition metal oxides (models **1**–**3**)

	Scheme	UHF	UB2VWN	US2VWN	UB2LYP	Exp.
CuOCu	$J_{ab}^{(1)}$	−218.1	−1666	−1874	−1476	
	$J_{ab}^{(2)}$	−219.5	−1800	−2041	−1576	
CuOCuOCu	$J_{ab}^{(1)}$	−79.71	−907.4	−1001	−785.4	−765 to −1049
	$J_{ab}^{(2)}$	−80.00	−939.2	−1042	−809.0	
Cu_4O_4	$J_{ab}^{(1)}$	−108.2	−468.8	−721.4	−514.9	−484 to −625
	$J_{ab}^{(2)}$	−145.0	−652.8	−1014	−717.2	
NiONi	$J_{ab}^{(1)}$	−49.28	−266.7	−358.3	−229.9	
	$J_{ab}^{(2)}$	−49.38	−278.4	−373.1	−238.7	
NiONiONi	$J_{ab}^{(1)}$	−43.04	−334.1	−383.3	−362.8	
	$J_{ab}^{(2)}$	−43.10	−339.1	−390.7	−368.5	
Ni_4O_4	$J_{ab}^{(1)}$	−36.47	−140.6	−156.5	−145.1	−139.0
	$J_{ab}^{(2)}$	−49.05	−190.9	−212.5	−196.2	

[a] J_{ab} are shown in cm^{-1}.

HH-type DFT methods such as UB2LYP and US2VWN are reliable enough for theoretical investigation of the effective exchange integrals in transition metal oxides, as in the case of transition metal halides [17]. This indicates an important role for EC in these species.

2.2. Effective exchange integrals for organic conductors

Recent experiments [19,20] have demonstrated that an AF phase exists near the superconducting state of the highest T_c organic superconductors; κ-(BEDT-TTF)$_2$X (X = Cu(NCN)$_2$ (**4**), Cu[N(CN)$_2$]Cl (**5a**), Cu[N(CN)$_2$]Br) (**5b**)). **4** and **5b** are superconductors at ambient pressure. On the other hand, **5a** is a paramagnetic insulator (PMI), but an antiferromagnetic insulating phase (AFI) is stabilized below $T_N = 27$ K at ambient pressure [19]. With increasing pressure, the Neel temperature of AFI is suppressed and the singlet superconducting phase (SSC) appears. The SSC transition temperature of **5a** takes its maximum value ($T_{SSC} = 13$ K) at 300 bar, but the SSC phase is also suppressed under high pressure, giving rise to a paramagnetic metal (PMM) phase. The phase diagram for **4**, **5a** and **5b** at ambient pressure [20] exhibits the same characteristic as that of cuprate superconductors [4].

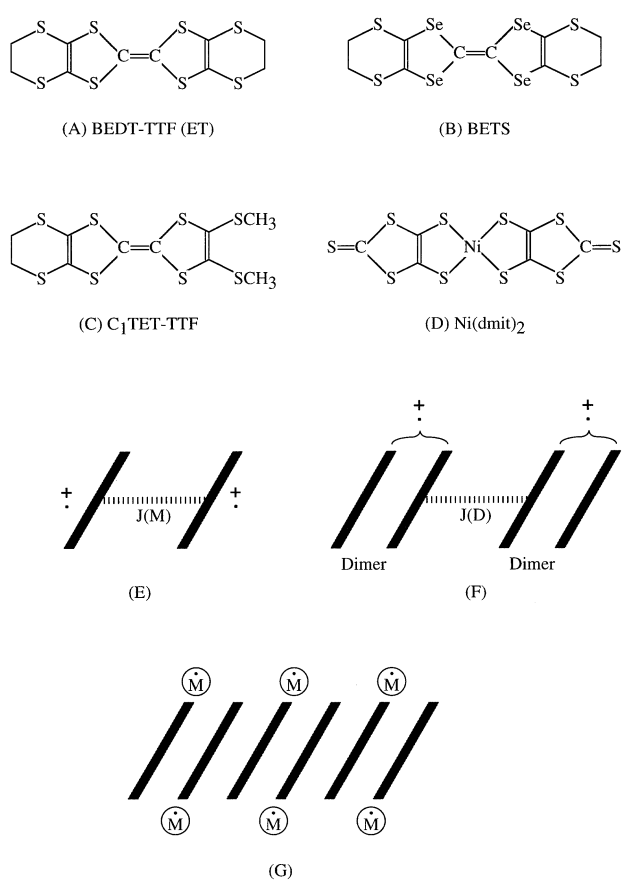

Fig. 2. Molecular structures of (A) BEDT-TTF(ET), (B) BETS, (C) C$_1$TET-TTF and (D) Ni(dmit)$_2$, (E) exchange interaction between monomer cation radical, (F) exchange interaction between dimer cation radical, and (G) organic conductors coupled with metal spins.

The extended Huckel band models usually provide Fermi surfaces for organic conductors constructed of BEDT-TTF and their derivatives, and simple band pictures have been used for qualitative explanations of the electronic properties of these complexes. However, Mott–Hubbard transitions often occur in organic charge-transfer complexes such as **5a**, β′-(BEDT-TTF)$_2$X (X = ICl$_2$, AuCl$_2$) (**6**) [21], λ-(BETS)$_2$-GaX$_z$Y$_{4-z}$ (**7**) [22], (C$_1$TET-TTF)$_2$Br (**8**) [21] and θ-(BEDT-TTF)$_2$RbZn(SCN)$_4$ (**9**) [23] at low temperatures, and the magnetic properties of these complexes are expressed by the Heisenberg model. Fig. 2 illustrates the molecular structures of BEDT-TTF(ET), BETS and C$_1$TET-TTF. The quasi-triangular lattice of (BEDT-TTF)$_2^+$ with one unpaired electron ($S = 1/2$) is formed in **5**, while the quasi-square lattices are formed in **6** and **7** as illustrated in Fig. 1. The triangular lattices of C$_1$TET-TTF and (BEDT-TTF)$_2^+$ are constructed in **8** and **9**, respectively. The intermolecular π–π interactions entail AF exchange interactions for **6** ($J_1 = -59$ K and $J_2/J_1 = 0.5$) and for **8** ($J_1 = -6.1$ K and $J_2/J_1 = 0.5$). The J values for **5** ($-J_1 > -J_2$), **7** ($-J_1 > -J_2 > -J_3$) and **9** ($-J_1 > -J_2 = -J_3$) are also negative as shown in Fig. 1.

As shown in Fig. 2E, we have calculated the J_{ab} (M) values between monomer cations (namely one-hole in each monomer (M)) of **4**, **5a**, **5b** and **5c** (X = Cu[N(CN)$_2$]I) by UB3LYP/6-31G, assuming the X-ray geometries of each dimer. The spin-projected scheme in Eq. (1) was used for comparison with other groups (see later). The J_{ab} (D) values between dimer cations (namely one-hole in each dimer) in Fig. 2F was simply estimated by assuming J_{ab} (D) = J_{ab} (M)/2. Table 2 summarizes the calculated results. The J_{ab} (M) values for the nearest neighbor pairs were smaller than -500 cm^{-1}, showing the strong HOMO–HOMO interaction. The exchange interactions in tetramers with two holes are approximately regarded as those between dimer cations with one hole as illustrated in **5**, **6**, **7** and **9** in Fig. 1. The calculated J_{ab} (D) values are in the range; -25–80 cm^{-1}, being compatible with the experimental values for **4**–**9**.

3. Hubbard and t–J models for strong electron correlation systems

3.1. Model Hamiltonians and electronic properties

In this section we briefly summarize the theoretical background for the molecular design of functional materials [5–9]. Previously, we have examined electronic structures of high-T_c copper oxides using ab initio MO

Table 2
Effective exchange integrals (J_{ab}) [a] calculated for dimer models of superconductors

X	J_1	J_2	J_3	Ref. [b]
κ-(BEDT-TTF)$_2$-Cu(NCS)$_2$ (**4**)	−101	−131	−111	[56]
	−111	−143	−124	[52]
	−61.0	−61.0	−35.5	Present [c]
κ-(BEDT-TTF)$_2$-Cu[N(CN)$_2$]Cl (**5a**)	−111	−111	−109	[52]
	−76.4	−76.4	−15.6	[53]
	−71.5	−71.5	−30.2	Present [c]
κ-(BEDT-TTF)$_2$-Cu[N(CN)$_2$]Br (**5b**)	−120	−120	−97.0	[52]
	−84.1	−84.1	−12.5	[53]
	−29.9	−29.9	−12.2	[54]
	−78.5	−78.5	−25.2	Present [c]
λ-(BETS)$_2$-GaX_2Y_{4-2} (**7**)	−91.0	−124	−24.2	[55a]
θ-(BETS-TTF)$_2$-$RbZn(SCN)_4$ (**9**)	−126	−28.3	−25.2	[55b]

[a] J_{ab} are shown in cm^{-1}.
[b] t, U and V are taken from these references.
[c] UB3LYP calculation.

methods [17,18], showing the necessity of N-band models for the systematic descriptions of magnetism, conductivity and superconductivity of the species as illustrated in Fig. 3. Some organometallic and organic systems isoelectronic to copper oxides have also been proposed on the basis of the ab initio results. N-band models also often reduce to the two-band model, which has been used for the elucidation of the Kubo–Inagaki [24,25] mechanism of ferromagnetism (FM) and other magnetic states, and the Suhl–Kondo mechanism [26,27] and related multi-band models [28–32] for superconductivity. In previous papers [33–36], the two-band model combined with the temperature Green function technique has been applied to elucidate phase diagrams of the charge density wave (CDW), spin density wave (SDW), singlet superconductivity (SSC), triplet superconductivity (TSC) and FM. The g-ology for the SSC phase is regarded as an extension of the Suhl–Kondo mechanism [26,27] for superconductivity. Instead of the two-band model, the Anderson lattice model [37] or the Kondo lattice model [38] can be used for theoretical descriptions of ferromagnetic metals, PMMs and spin liquid of electron- or hole-doped conducting polymers interacting with coordination compounds with spins ($M^{\bullet}$) [39,40] and donor (D)–acceptor (A) complexes, where D or A are interacting with the species ($M^{\bullet}$) [5,41]. The so-called RKKY model [42–44] is used for a theoretical description of the effective exchange coupling of spins via the spin polarization of the conduction electron. The RKKY model has been employed for theoretical studies of FM, AF, helical spin structure and spin glass of organic and organometallic magnetic materials.

3.2. Superconductivity by t–J model

Previously [33–35] the four-component spinor (Nambu expression) was introduced to characterize possible electronic phases of molecular materials: (1)

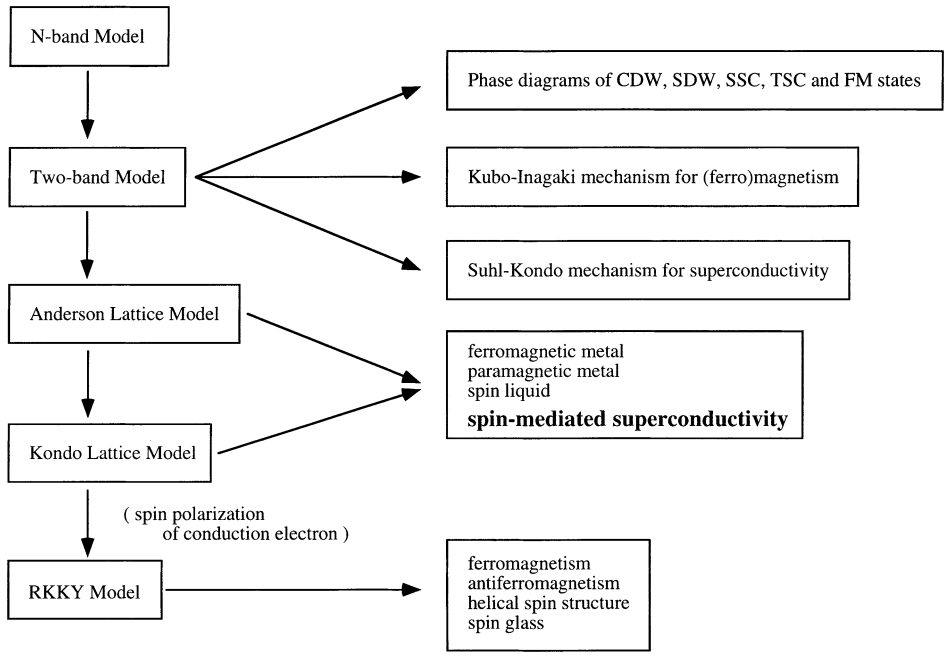

Fig. 3. Multi-bands Hubbard, Anderson and Kondo, and RKKY models for magnetic conductors and superconductors.

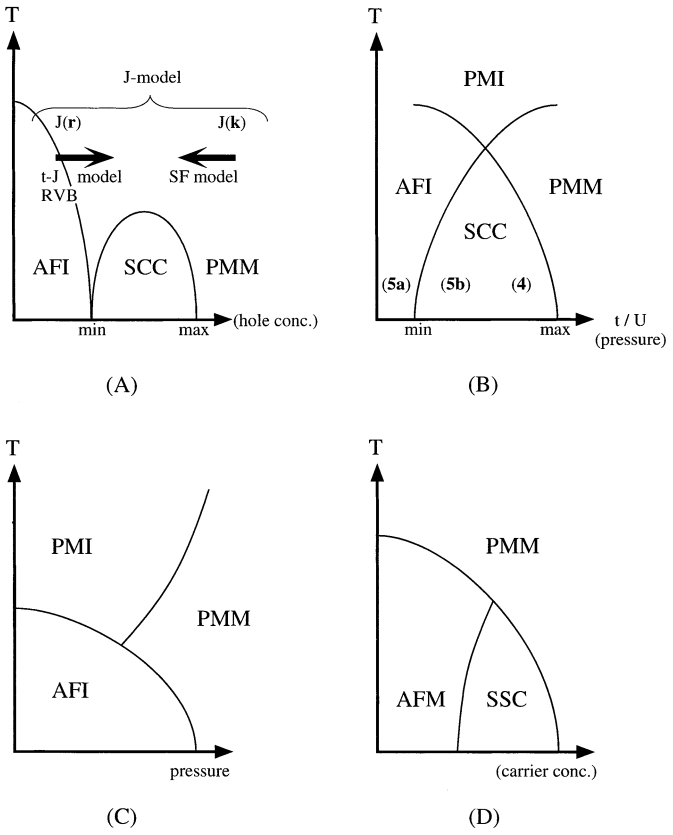

Fig. 4. Phase diagrams for strongly correlated electron systems: (A) copper oxides, (B) $(BEDT\text{-}TTF)_2X$, (C) V_2O_3 and (D) $(BETS)_2X$. Notations are given in text.

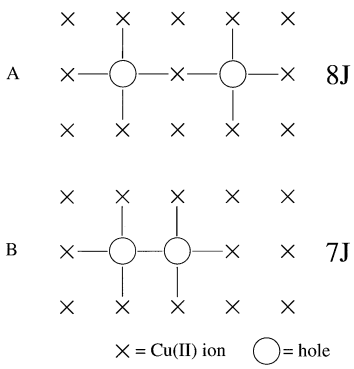

Fig. 5. Simple models (A, B) for Cooper pair formation via exchange interactions (J) in our J-model.

CDW, (2) SDW, (3) SSC, (4) TSC and (5) FM. The phase diagrams of these states were depicted using a two-band model in combination with the temperature Green function technique (see Fig. 3). Our theoretical investigations elucidated four different approaches to obtain high-T_c superconductors in the intermediate regime of the metal insulator transitions. One of them is an approach from the strong correlation limit using the resonating valence bond (RVB) and the other is a spin-fluctuation model from the metallic side: these were referred to as the unified J-model [5,36] as illustrated in Fig. 4A.

Our unified J model [6,41] was extended so as to reproduce experimental results on the basis of the Ginsburg–Landau (GL) model [33]. The transition temperatures for AF and SSC phase were given by

$$T_c(\mathrm{AF}) \propto J(x_{\min} - x) \tag{3a}$$

$$T_c(\mathrm{SSC}) \propto J(x - x_{\min})(x_{\max} - x) \tag{3b}$$

where x is the hole concentration, and $x_{\min}$ and $x_{\max}$ are its lower and upper limits for SSC. The T_c for AF phase decreases with the increase of x ($x < x_{\min}$), while T_c for SSC has the maximum in the intermediate region ($x_{\min} < x < x_{\max}$). The origin of the high-T_c superconductivity of copper oxides is regarded as a strong effective exchange interaction ($2|J| > 1000\ \mathrm{cm}^{-1}$) [5,17] as illustrated in Fig. 5. The eight J-bonds (8J) are lost when two holes are separated in 2D plane of copper oxides in Fig. 5A, while the seven J-bonds (7J) are broken in the case of the hole paired configuration in Fig. 5B. This implies that an attractive interaction between holes is J in our J-model [5,17]. This model at least works well for a simple explanation of the high-T_c superconductivity of copper oxides.

In order to confirm the simple picture above, exact diagonalizations [36] of Hubbard models have been performed for finite clusters. Recent numerical calculations [4] for the two-dimensional (2D) t–J model have been carried out to elucidate the relative stabilities among the AF state and several SSC states with different symmetries:

$$\Delta k = \begin{pmatrix} \Delta\text{: } s\text{-wave} \\ \Delta \sin k_x \sin k_y\text{: } d\text{-wave} \\ \Delta(\sin k_x + C \sin k_y)\text{: } (s+d)\text{-wave} \\ \Delta(\sin k_x + e^{i\theta} \sin k_y)\text{: } (s+id)\text{-wave} \end{pmatrix} \tag{4}$$

where the k-space representation is used instead of the site representation in Eq. (4). The states with $C = 1$ and $C = -1$ denote, respectively, the extended s-wave and pure $d_{x^2-y^2}$ (d) wave and the state with $q = p/2$ means the $(s + id)$-state. At the half-filling state (no-hole), the AF state is more stable than the SSC state with the $d_{x^2-y^2}$ (d) symmetry, though the latter is the most stable among the SSC states in Eq. (4). On the other hand, the $d_{x^2-y^2}$ (d) wave SSC state becomes the ground state in the approximate hole-doped region, in accord with the experiment [4]. Interestingly, the kinetic energy (t) does not favor superconductivity in all the hole-doped region. The exchange term (J) gives the attractive force in the $d_{x^2-y^2}$ (d) channel, supporting our J-model [5,9].

In fact, the energy gap in Eq. (4) is numerically given by $\Delta = 0.15J - 0.27J$ [4] ($= 1.13\ T_c$ by the BCS theory), supporting Eq. (3b). The T_c can be estimated easily by

inserting the ab initio J_{ab} values in this relationship, providing that $T_c = 100$–150 K [28]. The estimated values are consistent with the experiments for high-T_c copper oxide superconductors. Thus ab initio J_{ab} calculations followed by the exact diagonalization of t–J model is useful for theoretical studies of superconductivity in strong correlation systems. However, it is noteworthy that there are many field-theoretical concepts [45] related to the t–J model such as non Fermi liquid, confinement and interlayer hopping. These are fully examined in Anderson's book [46]. It is noteworthy that our J model in Fig. 4A [17,28] was independently introduced from the t–J model so as to express ab initio results in terms of spin correlation functions in both real and k-spaces.

3.3. Spin mediated models for superconductivity

The high-T_c cuprate superconductors were fully examined on the basis of ab initio computational results and Hubbard [47] models [5,9,41]. They are also investigated by the band models by the use of Green function techniques [33–36]. The spin-mediated or EC models from both AF and metallic sides in Fig. 4 work well for a qualitative understanding of the high-T_c superconductivity. More reliable computations involving higher-order correlations such as fluctuation exchange (FLEX) approximation [48–51] also indicated that spin fluctuation effects play an important role for high-T_c superconductivity. Recent experimental results [4] are not inconsistent with these theoretical results.

Recently, spin-mediated superconductivity has also been proposed for organic conductors and superconductors mentioned above. Both ab initio and semiempirical calculations [52–55] have been performed to determine reasonable parameters for the Hubbard models for **5a**. The Hubbard models for **5a** and related species such as α-(BEDT-TTF)$_2$I$_3$ were solved by the mean field approximation to reproduce the experimental phase diagram given in Fig. 4B [56]. For comparison, the three-dimensional (3D) Mott insulator V_2O_3 is depicted in Fig. 4C, where a superconducting phase does not appear because of 3D lattice dimensionality [4]. This in turn implies an important role of 2D character for cuprate and organic superconductors. The anisotropic triangular lattice Hubbard model for **5a** was investigated by the FLEX method, which can treat AF and superconductivity (SSC) on equal footing, and it was shown that d-wave SSC is realized in a wide region of the phase diagram next to the AF phase [57]. The dynamical susceptibility and self energy for a simplified dimer Hubbard model were calculated by FLEX, and T_{SSC} obtained by solving the linearized Elishberg type equation was in good agreement with the experiment [58]. The third-order correction was also examined to confirm the spin fluctuation mediated superconductivity for **5a** [59]. The multicritical phenomena of SSC and AF for **5a** were analyzed in terms of the renormalization and SO(5) symmetry groups [31,60], suggesting that the origin of the SSC with d-wave symmetry is common with that of the AF.

All these advanced theories [52–60] indicated an important role for EC effects for SSC and AF of **5a**. In fact, we can reproduce the phase diagram in Fig. 4B for **5a**, assuming that the transition temperatures (T_c) for superconductivity are given by Eq. (3b), while T_c for AF and nonmagnetic insulating (NMI) phases for **5a** and **7**, respectively, are given by

$$T_c(\text{AF or NMI}) \propto J(x_{max} - x) \tag{3c}$$

Note that Eq. (3c) is equivalent to that of spin gap (SG) phase for cuprate superconductors [33]. So, here we apply our J-model [17] even for organic superconductors.

To this end, we have calculated J_{ab} values using transfer integrals (t) and on-site repulsion integral (U) in Refs. [52–60], assuming the dimer model as:

$$J_{ab} = -\frac{2t^2}{U} = -\frac{2s_{ab}^2\beta^2}{U} \tag{5}$$

where s_{ab} denotes the SOMO–SOMO overlap integral between cation radicals of BEDT-TTF and β is the resonance integral parameter. The β- and U-parameters were calculated by UHF and hybrid DFT/6-31G* methods. Table 3 summarizes the calculated results. The β-values are not so different among the methods, while the U-values are different. The U-values by UHF and UBLYP are too large and too small, respectively. The $|J_{ab}|$ values by UB2LYP are smaller than the experiments, in sharp contrast to those of copper and nickel oxides. In fact, the J_{ab} values for **4**, **5a**, **5b**, **7** and **9** by our B3LYP calculations in Table 2 are compatible with those of ab initio methods by other groups [52,54]. This means that these organic systems belong to the intermediate correlation regime. However, it is noteworthy that the J_{ab} values by semiempirical methods are larger than the ab initio values as shown in Table 2.

Interestingly, ab initio calculations predict that the magnitude of J_3 is rather small, and therefore the magnetic structure of **4** and **5** should be regarded as a square planar lattice similar to the cuprate superconductors, though the semiempirical calculations show the triangular lattice. If we assume the J-model of copper oxides for T_{SSC}, $\Delta = 0.10J - 0.15J$ [5] ($= 1.13$ T_c by the BCS theory), the estimated T_{SCC} is in the experimental order because $J = -5$ to 15 K for **5**–**9**. This in turn indicates that the spin fluctuation mechanism may be operative for organic superconductors **5** and **7**.

Table 3
All effective magnetic parameters evaluated with parameter fitting for dimer structure in κ-phase crystal of BEDT-TTF and BETS

	J_{ab} (cm^{-1})	s_{ab}	t_{ab} (eV)	β (eV) [a]	U_{eff} (eV) [a]	x [b]	
UHF/6-31G	−280	0.0324	0.168	5.19	1.68	0.1	
UB2LYP	−479	0.0334	0.141	4.21	0.603	0.234	
UB3LYP	−693	0.0338	0.152	4.50	0.374	0.406	
UBLYP	−1004	0.0337	0.147	4.36	0.138	1.07	
RHF	−436		0.269		2.68	0.100	Imamura
Hubbard	−1065	0.026	0.26	10.0	0.78	0.333	Kino

[a] The J and s values are calculated for all pairs in all complexes and are employed in order to evaluate effective parameters.
[b] $x = (t_{ab})/(U_{eff})$.

4. Magnetic conductors and superconductors via π–d interactions

4.1. Anderson and Kondo lattice models

As shown in Fig. 3, molecular systems described by multi-band models are our theoretical targets to realize multifunctional materials. Previously we have used Anderson and Kondo lattice models [5,61] for the molecular design of doped-magnetic polymers and segregated columns of CT complexes coupled with coordination compounds with spins ($M^{\bullet}$) as illustrated in Fig. 2G. Very recently, AF and ferromagnetic metal states were discovered for organic–inorganic hybrid systems such as $(BEDT\text{-}TTF)_2Y$ and $(BETS)_2Y$ ($Y = Fe(III)X_4$ (X = halogens, etc.)). The Anderson model Hamiltonian for these species is given by

$$\begin{aligned} H &= \sum \varepsilon_{\mathbf{k}} c^{\dagger}_{\mathbf{k}\sigma} c_{\mathbf{k}\sigma} + \sum E_M M^{\dagger}_{i\sigma} M_{i\sigma} + U \sum_i M^{\dagger}_{i\uparrow} M_{i\uparrow} M^{\dagger}_{i\downarrow} M_{i\downarrow} \\ &\quad + T \sum_{i\sigma} (M^{\dagger}_{i\sigma} c_{\mathbf{k}\sigma} + c^{\dagger}_{\mathbf{k}\sigma} M_{i\sigma}) \\ &= \sum \varepsilon_{\mathbf{k}} c^{\dagger}_{\mathbf{k}\sigma} c_{\mathbf{k}\sigma} + \sum E_M M^{\dagger}_{i\sigma} M_{i\sigma} \\ &\quad + \frac{U}{N_0} \sum_{\mathbf{k},\mathbf{k}',q} M^{\dagger}_{\mathbf{k}+q\uparrow} M^{\dagger}_{\mathbf{k}'-q\downarrow} M_{\mathbf{k}'\downarrow} M_{\mathbf{k}\uparrow} \\ &\quad + T \sum_{\mathbf{k}\sigma} (M^{\dagger}_{\mathbf{k}\sigma} c_{\mathbf{k}\sigma} + c^{\dagger}_{\mathbf{k}\sigma} M_{\mathbf{k}\sigma}) \end{aligned} \quad (6)$$

where ε_k is the energy level of the conduction electron and U and E_M denote the on-site Coulomb repulsion of spin site ($M^{\bullet}$) and SOMO energy level of $M^{\bullet}$, respectively, and T is the interaction matrix element between conduction electron and SOMO electron. $M_{i\sigma}$ and $M_{k\sigma}$ are annihilation operators with spin σ at the i-th site and with momentum k and spin σ, respectively. The electronic structures of the Anderson lattice model are highly dependent on the relative magnitudes of $\varepsilon_{\mathbf{k}}$, E_M and U as illustrated in Fig. 6. The spin sites ($M^{\bullet}$) are oxidized into the cationic states (M^{+}) if $E_M \gg \varepsilon_F$ (Fermi level of conduction band) in the case of Fig. 6A, while they are reduced to the anionic sites (M^{-}) if $\varepsilon_F \gg E_M$ for the case of Fig. 6B. The unpaired electrons on the spin sites are lost in these situations, leading to PMM states. On the other hand, the mixed valence (MV) states become feasible if $\varepsilon_F = E_M$ as shown in Fig. 6C. The average (uniform) net charge ($0 < Q < 1$) on radical sites should be observed because of resonance between neutral $M^{\bullet}$, ($Q = 0$) and oxidized M^{+}, ($Q = 1$) configurations of radical sites in the case of the MV type III state. Similarly, the MV type III state ($-1 < Q < 0$) may be possible if $\varepsilon_F = E_M + U$ as shown in Fig. 6D, where neutral $M^{\bullet}$ ($Q = 0$) and anionic M^{-} ($Q = -1$) configurations of radical sites are resonating. The SOMO electrons on the radical sites are delocalized over whole lattices, giving metallic states in the MV type III situations.

The so-called Kondo regime [38,61,62] is defined as a specific state where the SOMO level (ER) is deeper than

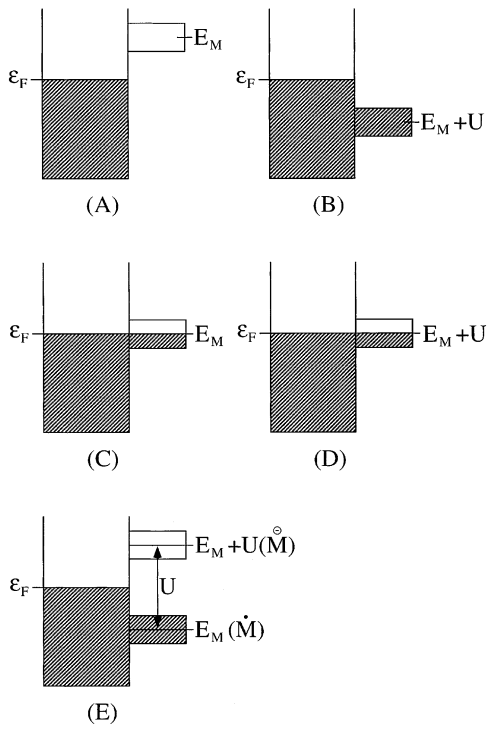

Fig. 6. Five different electronic configurations (A–E) for the Anderson lattice Hamiltonian for organic/inorganic hybrid systems.

the Fermi level (ε_F), even if the band width (Γ) of radical electrons is taken into account ($\varepsilon_F - E_M \gg \Gamma$), where $E_M + U - \varepsilon_F \gg G$ because of the strong on-site repulsion U of radical sites as illustrated in Fig. 6E. This implies that subtle balances of Fermi (HOMO) levels of conducting polymers (or CT complexes) and SOMO levels of coordination compounds, together with Coulomb repulsion (U) for spin sites are necessary for achievement of the Kondo regime. In fact, we have examined the energy levels of TTF-spin ($M^{\bullet}$) systems by ab initio calculations and have shown that such a situation can be realized in the system [39,40,62].

In this situation, spins on the spin sites are alive under physical doping to generate conduction electrons in the field effect transistor (FET) configuration [63]. Therefore, several spin-mediated electronic states such as ferromagnetic metal and spin mediated superconductivity are expected in the Kondo regime. The slave boson method, which eliminates the double occupancy of radical states (see Ref. [40]), can be used to solve the Anderson lattice model [37] to depict the phase diagram. Some SOMO electrons on radical sites are almost localized in the Kondo regime, only their spin freedom remains, leading to the Kondo lattice model as follows

$$H_{KM} = \sum_{\mathbf{k}\sigma} \varepsilon_{\mathbf{k}} c^{\dagger}_{\mathbf{k}\sigma} c_{\mathbf{k}\sigma} + J_{CM} \sum \boldsymbol{s}_i \cdot \boldsymbol{S}_i \tag{7}$$

where $\boldsymbol{S}_i$ means spin localized at radical site i and $\boldsymbol{s}_i$ denotes the spin density of conduction electron at site i

$$\boldsymbol{s}_i = \frac{1}{2} \sum_{\sigma\sigma'} c^{\dagger}_{i\sigma} \tau_{\sigma\sigma'} c_{i\sigma'} \tag{8}$$

where $\tau = (\tau_x, \tau_y, \tau_z)$ is the Pauli spin matrix. The Kondo lattice model has been used for molecular design of organic Kondo and dense Kondo systems [62].

Since localized spin $\langle \boldsymbol{S}_i \rangle$ at site i induces the local magnetic field ($-J_{CM}\langle \boldsymbol{S}_i \rangle$) on conduction electrons, the spin polarization on site j is given by

$$\langle S^{\alpha}_j \rangle = -J_{CM} \sum_{\beta = x,y,z} \chi^{\alpha\beta}(j, i) \langle S^{\beta}_i \rangle \tag{9}$$

where $\chi_{ab}(j, i)$ denotes the local magnetic susceptibility. Then the magnetic interaction of localized spin $\langle \boldsymbol{S}^{\alpha}_j \rangle$ at site j with $\langle \mathbf{S}^{\beta}_j \rangle$ is defined by

$$H_{RKKY} = -J^2_{CR} \sum_{\langle ij \rangle} \sum_{\alpha\beta} S^{\alpha}_j \chi^{\alpha\beta}(j, i) S^{\beta}_i \tag{10a}$$

$$= -2J_{ij} \sum_{\langle ij \rangle} \boldsymbol{S}_j \cdot \boldsymbol{S}_i \tag{10b}$$

where

$$\frac{1}{2} J^2_{CR} \chi^{\alpha\beta}(j, i) = J_{ij} \delta_{\alpha\beta} \tag{11}$$

Thus the exchange coupling between radical spins via the spin polarization of conduction electrons is described by the RKKY type spin Hamiltonian [42–44]. The RKKY model has been used for the molecular design of several magnetic states of magnetic polymers and crystals [5,61,62].

4.2. Molecular design of π–d interaction systems

Previously [5], we have theoretically examined possible organic, organometallic analogs to copper oxides and magnetic conductors on the basis of both ab initio and Hubbard model calculations. In fact, several strategies are presented: (1) magnetic modification of conducting polymer [6–8], (2) magnetic modification of TTF BEDT-TTF and BETS derivatives, (3) magnetic modification of Ni(dimt) systems in Fig. 2D [40], and (4) construction of organic RVB [61]. During this past decade, experimental results concerning the proposal (2) have been reported. We wish to discuss these results in relation to our theoretical models proposed previously [5,17,28–31].

4.2.1. Organometallic RKKY systems and spin-mediated superconductors

Since the direct introduction of a radical group into BEDT-TTF, BETS and Ni(dimt)$_2$ molecules in Fig. 2 are not so easy [62–66], transition metal complexes with spin(s) such as Fe(III)X$_4$ (X = Cl, Br, I) would be used so as to couple with conduction electron [67,68]. The synthesis of organic–inorganic hybrid layer systems is now receiving considerable interest in relation to possible electronic phases as illustrated in Figs. 2G and 7A. Active control of π–d levels by experimental procedures is essential to induce strong through-space effective exchange coupling (J_{ai}) between the conduction electron and spin. However, organic layers often exhibit the Mott transition, giving rise to AF insulators such as **5a** and **6** as shown in Fig. 7B. While organic metals (M) or superconductors (SSC) are realized, such as **5b** in Fig. 7C, if the Mott transition to AFI is suppressed. On the other hand, the SSC state is suppressed if localized spins in insulating phase are intercalated as shown in Fig. 7D. Recently, several interesting systems have been presented (see below).

Mallah et al. [69] and Kurmoo et al. [70] have investigated π–d interactions in (BEDT-TTF)$_2$FeX$_4$ (X = Cl or Br). The magnetic susceptibility data of these compounds are fitted well to the Weiss law

$$\chi = \chi_0 + C/(T - \theta) \tag{12}$$

where C and θ are the Curie constant and Weiss temperature, respectively. The Weiss temperatures were -6 and -5 K for FeCl$_4$ and FeBr$_4$ salts, respectively. Figs. 2G and 8 illustrate the superexchange interactions of spins of transition metal ions via donor groups; ↑Fe(III)–X···(BEDT-TTF)$_2$···X–Fe(III)↓. This means a weak AF superexchange interaction between Fe(III)

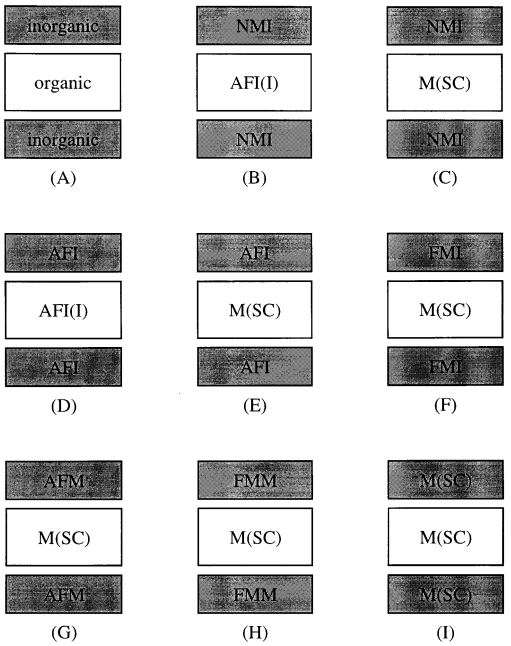

Fig. 7. Possible electronic structures (A–I) of organic/inorganic layered materials. The notations of NMI, AFI, FMI, M, AFM, FMM and SC are given in text. Examples of A–G are shown in this review but H and I are not synthesized yet.

spins through (BEDT-TTF)$_2$. Day et al. [71] investigated a composite system composed of BEDT-TTF and copper complexes; (BEDT-TTF)$_3$CuCl$_4$·H$_2$O. The exchange coupling constant between the conduction electron and Cu(II) localized spin in this organic–inorganic composite system is rather small because of nearly zero orbital overlap, showing no exotic phenomena arising from the π–d interaction. Similarly, the π–d effective exchange interaction was weak in the case of the Coronado composite system; (BEDT-TTF)$_8$5.5(H$_2$O)-[CoW$_{12}$O$_{40}$] [72]. The exchange interaction between conduction electron and spin was also weak in this case. Recently Enoki and his collaborators [73] and Marsdon et al. [74] investigated (BEDT-TTF)$_3$CuBr$_4$ and (BEDT-TTF)$_3$CuBr$_2$Cl$_2$ solids and found that the intralayer AF exchange interaction (J_{dd}) between 1/2 spin of copper ion (see Eq. (10)) is -12 cm^{-1} for the former and the AF transition of Cu(II) layers occurs at $T_N = 7.65$ K. These complexes exhibit a metallic behavior under high pressure and behave as p–d Kondo systems, which are expected as described in Section 4.1. Their results indicate that spin delocalization of the Cu(II) 3d spin over the Br 4p orbital is essential for the RKKY interaction via Br and BEDT-TTF orbitals contact. Both crystal and orbital engineering approaches are necessary for controlling the RKKY interaction.

Kurmoo et al. found coexistence of the magnetism and superconductivity in the (BEDT-TTF)$_4$(H$_2$O)-Fe(C$_2$O$_4$)$_3$·C$_6$H$_5$CN composite system [75]. Very recently, Kobayashi et al. [76–82] found that a series of λ- and κ-(BETS)$_2$MX$_4$ systems (MX$_4$ = GaCl$_4$, FeCl$_4$, FeBr$_4$, (Fe$_x$Ga$_{1-x}$)Cl$_4$ and FeBr$_x$Cl$_{1-x}$) exhibit metal-insulator transitions, superconductivity, coexistence of superconductivity and AF, and other electronic properties. For example, λ-(BETS)$_2$GaCl$_4$ and λ-(BETS)$_2$-FeCl$_4$ exhibited, respectively, a superconductivity transition at $T_{SSC} = 8$ K (Fig. 7B), and a coupled metal-insulator and AF transition at 8.5 K (Fig. 7C). The localized spin of Fe(III) ion ($S_a = 5/2$) clearly suppressed the superconductivity. The hybrid systems, λ-(BETS)$_2$(Fe$_x$Ga$_{1-x}$)Cl$_4$ and (BETS)$_2$FeBr$_x$Cl$_{1-x}$ indicated interesting mixed electronic and magnetic properties, which were highly sensitive to the concentration x, external pressure and other structural factors. Meanwhile, κ-(BETS)$_2$FeBr$_4$ was an antiferromagnetic organic metal (AFM) at ambient pressure ($T_N = 2.5$ K) (Fig. 7D), showing the existence of π–d interaction between conduction electron and Fe(III) spin. Moreover, the heat capacity experiment suggested the coexistence of the superconductivity and AF long-range order below $T_{SSC} = 1$ K. The same situations appeared in the case of κ-(BETS)$_2$FeCl$_4$, though the corresponding phase transition temperatures are low; $T_N = 0.65$ K and $T_{SSC} = 0.1$ K, respectively. Fig. 4D illustrates the phase diagram for the species.

The complex phase transitions of λ- and κ-(BETS)$_2$MX$_4$ systems are qualitatively understood in terms of the generalized Kondo model describing π–d interactions in section Section 4.1 [5,61–63]. For example, Brossard et al. [78] showed that the effects of a RKKY-type indirect exchange and of applied magnetic field are described within the framework of a generalized Kondo lattice model, namely two chains of $S = 5/2$ Fe(III) localized spins coupled through the itinerant spins of 2D sheets of BETS in λ-(BETS)$_2$FeCl$_4$ as illustrated in Fig. 7D. Hotta and Fukuyama [83] have made extensive numerical studies of λ- and κ-(BETS)$_2$MX$_4$ systems on the basis of the generalized Kondo Hamiltonian and have depicted various phase diagrams under the mean field approximations [83]. Their results are qualitatively consistent with available experiments.

Coronado et al. [84] have proposed strategies for creating bifunctionality targets, hybrid organic/inorganic crystals comprising two functional sublattices exhibiting distinct properties. In this way, they recently found coexistence of FM and metallic conductivity in [BEDT-TTF]$_3$[Mn(II)Cr(III)(C$_2$O$_4$)$_3$] composite crystals (Fig. 7E). The transition metal ions form a honeycomb bimetallic network which exhibit the ferromagnetic transition at $T_F = 5.5$ K. There is no strong interaction between the ferromagnetic network and (BEDT-TTF) sheets, showing essential decoupling between the sublattices.

4.2.2. Ab initio calculation of $J_{\pi d}$ values

Experimentally, the exchange coupling constants between conduction electron and Fe(III) spin are in the range: -8 to -23 K. Judging from T_N for AF order, the magnitude should become large in the case of $FeBr_4$ salts. Thus, the π–d interaction increases in the following order:

$$FeCl_4 \rightarrow FeBr_xCl_{1-x} \rightarrow FeBr_4 \quad (13a)$$

$$\text{BEDT-TTF} \rightarrow \text{BETS (substitution of 4S with 4Se)} \quad (13b)$$

These tendencies are reasonable from the viewpoint of spin delocalization in MX_4 and intermolecular orbital overlap. Experimentally, $(BEDT\text{-}TTF)_2FeX_4$ (X = Cl or Br) is an antiferromagnetic insulator (AFI), while $(BETS)_2FeX_4$ (X = Cl or Br) is antiferromagnetic metal (AFM). This implies that metallic character is predominant for BETS salts. Fig. 4D illustrates the coexistence of AFM and SSC for these species. If we apply the J-model from the metallic side (J_Q in Fig. 4A) [28], the origin of SSC should be spin-fluctuation instead of electron–phonon interaction, though a cooperative mechanism of electron–phonon and spin fluctuation is another possibility [5]. Judging from the small $|J_{ab}|$ values ($|J| < 10$ cm^{-1}), the transition temperature for spin-mediated superconducting should be low ($T_c \approx 1$ K).

In order to examine the above picture, we have performed ab initio calculations of the effective exchange interaction between ($J_{\pi d}$) cation radical of BETS and Fe(III)X_4 as illustrated in Fig. 8. The $J_{\pi d}$ values evaluated by the UHF method with the MIDI ((53321/53/41) + 4p, for Fe) and 6-31G (for others) basis sets are -0.101, -3.64 and -5.61 cm^{-1} for $BETS^+$ (1/2↑ or 1/2↓)···$FeCl_4$(5/2↑) [= direct], BETS(0)···BETS(1/2↑ or 1/2↓)···$FeCl_4$(5/2↑) [= close-spins] and $BETS^+$ (1/2↑ or 1/2↓)···BETS(0)···$FeCl_4$(5/2↑) [= end-spins], respectively. From these results it is found that the $J_{\pi d}$ values are very small but AF though the magnetic interactions in the two latter models cannot be negligible.

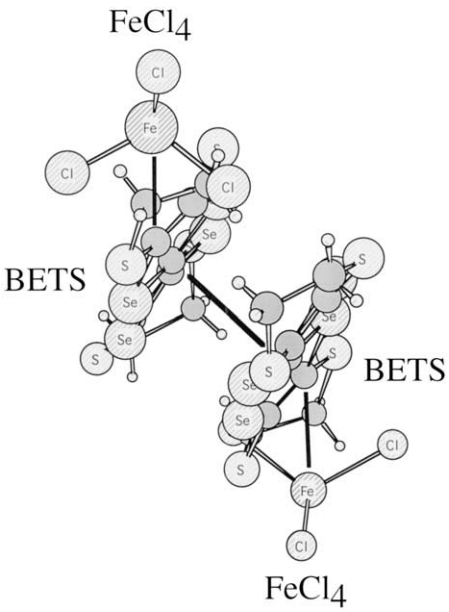

Fig. 8. Computational model for the effective exchange interaction between cation radical of BETS and Fe(III)X_4.

Through-space π–d interactions are usually weak in the pendant type composite systems. Therefore, the backbone-type complexes are other targets for magnetic conductors and superconductors. The composite π–d systems involving copper ion synthesized by Gatteschi et al. [85] and Kitagawa and Munakata group [86] indicated a weak π–d interaction in the main chains. On the other hand, transition-metal tetrathiolate polymers synthesized by us [40] showed strong superexchange interactions, though single crystals were not obtained. Thus, spin–spin interactions become relatively strong in the backbone-type π–d conjugated systems. In the future, experimental efforts in this direction may provide the two leg ladders and related systems with higher transition temperatures.

4.2.3. Spin frustrated systems

After the discovery of high-T_c superconductivity [1], triangular spin systems have attracted great interest because of Anderson's RVB theory [87,88] for magnetism and superconductivity. Many field theoretical models [89] have been presented for the high-T_c superconductivity in conformity with Anderson's proposal. Instead of the through-bond approach to construct spin frustrated systems [36,88,89], the through-space approach is rather simple since many radicals and ion-radicals can be used for component units. For example, three-center units (**1**), nitronyl nitroxide (NN) derivatives, doped BEDT-TTF and BETS molecules, etc. would be building blocks for organic spin frustrated systems.

Awaga et al. [90] have discovered the organic Kagome system (see **8** and **9** in Fig. 1) composed of p-MPNN, which does not exhibit magnetic ordering even at low temperature because of strong spin frustration. The introduction of carrier into this system seems difficult. Enoki et al. [49] also found the triangular lattice composed of the BEDT-TTF plus Br complex (**8** in Fig. 1). Their results for the complex showed peculiar magnetic behaviors. Recently several theoretical studies have been carried out to elucidate the possibility of *d*-wave superconductivity in doped triangular lattices [87–89].

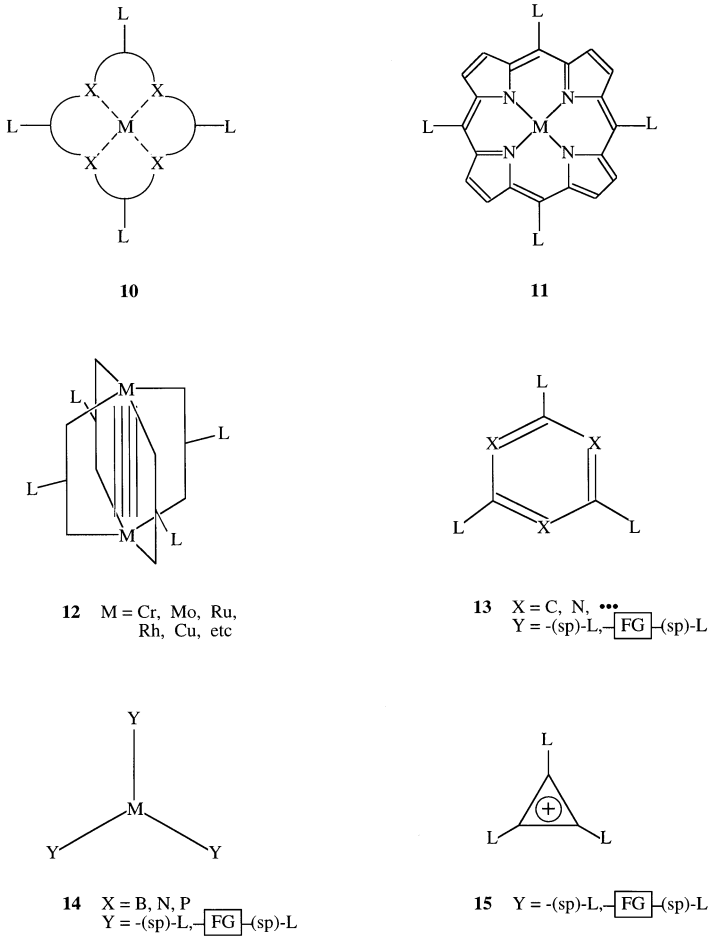

Fig. 9. Metal complexes with four (**10**–**12**) and three (**13**–**15**) hands for units of constructions of square planar and triangular lattices.

5. Outlook

5.1. Constructions of 2D structure

According to the aforementioned theoretical and experimental results we wish to refine previous models of extended organic–inorganic hybrid systems [5,6]. The key points are constructions of well-organized networks of transition metal ions, functional groups and other components. Fortunately, many strategies for the construction of such networks have been developed in the past decade by several groups [91–99]. Fig. 9 illustrates component units with four hands (L: ligands) to construct two-dimensional (2D) lattices: (a) chelating compounds (**10**), (b) porphyrin compounds (**11**) and (c) Cotton-type binuclear complexes (**12**). Some 2D lattices were already constructed by using Cotton-type binuclear transition metal complexes by Yagi et al. [91,92] and Mori et al. [95] as illustrated in Fig. 10. Benzene and other hydrocarbons substituted with $(COO^-)_2$ groups and other organic ligands were used to construct nanopores for gas occlusion in their cases. Here, we want to construct the square planar lattices which are isoelectronic to the CuO_2 plane in copper oxide superconductors. For this purpose, various electron donors or acceptors are utilized as functional groups, for which a hole or electron is introduced such as the hole- or electron-doped CuO_2 plane. If necessary, dopants are introduced in the pores as shown in Fig. 10A. Ferrimagnetic or ferromagnetic conductors might be realized if metal sites have spins like mixed-valence binuclear systems. The transition metals coordinated by linking ligands are regarded as junctions for lattice constructions in these cases, like nanopore systems. Spin-mediated superconductivity might be realized in special cases, for which large spin fluctuations and strong effective exchange interactions are realized in the 2D lattices.

5.2. Constructions of spin-frustrated structures

The introduction of electron carriers into spin frustrated systems is one possible way to spin-mediate superconductors in Fig. 2. The RVB state with spin frustration is expected to be a possible precursor for this purpose. Triangular spin lattices and other non-

collinear spin lattices such as Kagome lattice in Fig. 1 are regarded as possible candidates for the organometallic RVB states. We have considered possible organic and organometallic spin frustration systems such as triangular ladder (**9**) and Kagome ladder (**8**) in relation to the RVB model for copper oxides as illustrated in Fig. 1. Recent experiments by Yaghi [91,92] and Williams [99] clearly demonstrated that the triangular and hexagonal lattices can be constructed using tridentate ligands (**13**) as shown in Fig. 9. Other tridentate organic ligands (**14**) and trinuclear complexes (**15**) are also utilized for constructions of these lattices. Therefore, we may construct spin frustrated systems by using functional groups with three coordination groups or triangular transition metal complexes with functional groups as illustrated in Fig. 9. Judging from the theoretical background described in previous [5,100] and present papers, the design and synthesis of spin frustrated lattices (B and C) and spin frustrated dendrimers (D and E) in Fig. 10 would be interesting for many reasons. For example, we may expect several exotic electronic states in Fig. 3. TTF, BEDT-TTF and BETS derivatives and other electron donors in Fig. 2 are utilized as functional groups introduced in the lattices. Spin dendrimers with fractal dimensions such as 2.5 dimension [101] would be realized because of recent developments in their synthetic methods. Thus, the through-bond approach is an alternative and promising strategy for the construction of spin frustrated systems.

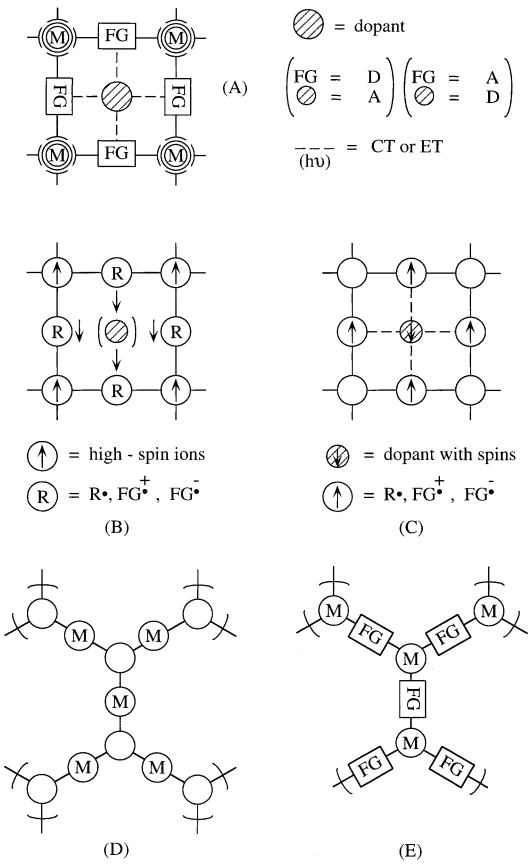

Fig. 10. Square planar and triangular lattices constructed of transition metal complexes and organic functional groups (FG) such as BEDT-TTF.

5.3. Active control of superconductivity by external fields

External magnetic field and magnetic impurities usually suppress or destroy SSC [1–4]. Similarly, the local spins of the FeX_4 magnetic anion should suppress the superconductivity of organic conductors such as λ-$(BETS)_2FeX_4$ and κ-$(BETS)_2FeX_4$ (X = Cl, Br). Very recently, it was found that λ-$(BETS)_2FeCl_4$ undergoes a transition from an AF insulator to a superconductor via a metallic state as an external magnetic field is increased [102]. The magnetic field due to the AF π–d exchange interaction with the Fe(III) ion could be compensated by the external magnetic field acting on the electron spins, leading the magnetic-field-induced superconductivity (FISC). This compensation is referred to as the Jaccarino–Peter (JP) effect [103,104]. Our ab initio calculations (see Section 4.2.2) show that the JP effect is equally expected for κ-$(BETS)_2FeX_4$ (X = Cl, Br), since the calculated J values are negative (AF). However, other effects such as orbital effects may contribute to the FISC. Further experimental and theoretical investigations are necessary for a complete understanding of its mechanism. Moreover, instead of the JP effect, spin fluctuation effects associated with magnetic ions with $S = 1/2$ such as Cu(II) and Ni(III) are also interesting in relation to the spin fluctuation mechanism [5,48–51] of copper oxide and organic superconductors.

The above example indicates the possibilities for the active control of superconductivity by external electronic and magnetic field [33–36]. In fact, photo-induced superconductivity has been realized for copper-oxide superconductors [105]. Synthetic efforts toward various coordination compounds responsible for external fields are very important for the development of molecular electronic devices.

Acknowledgements

This work has been supported by Grants-in-Aid for Scientific Research on Priority Areas (No. 401, "Metal Assembled Complexes") from the Ministry of Education, Science, Sports, and Culture, Japan. K.Y. thanks Professors H. Fukutome, W. Mori, K. Nasu, S. Miyashita, N. Suzuki, Y. Kitaoka and Y. Nakazawa for their helpful discussions.

References

[1] J.G. Bednort, K.A. Muller, Z. Phys. 64 (1986) 189.
[2] A.P. Kampf, Phys. Rep. 249 (1994) 219.
[3] W. Brenig, Phys. Rep. 251 (1995) 153 and references therein.
[4] M. Imada, A. Fujimori, Y. Tokura, Rev. Mod. Phys. 70 (1998) 1040.
[5] K. Yamaguchi, Int. J. Quant. Chem. 37 (1990) 167.
[6] K. Yamaguchi, Y. Toyoda, T. Fueno, Kagaku 41 (1986) 585 in Japanese.
[7] K. Yamaguchi, Y. Toyoda, T. Fueno, Synth. Met. 19 (1987) 81, 87.
[8] K. Yamaguchi, M. Nakano, T. Fueno, Kagaku 42 (1987) 583 in Japanese.
[9] H. Nagao, M. Nishino, Y. Shigeta, T. Soda, Y. Kitagawa, T. Onishi, Y. Yoshioka, K. Yamaguchi, Coord. Chem. Rev. 198 (2000) 265.
[10] P. Bourges, H. Casalta, A.S. Ivanov, D. Petitgrand, Phys. Rev. Lett. 79 (1997) 4906.
[11] S. Shamoto, M. Sato, J.M. Tranquada, B.J. Sternlieb, G. Shirane, Phys. Rev. B48 (1993) 13187.
[12] T. Ami, M.K. Crawford, R.L. Harlow, Z.R. Wang, D.C. Johnston, Q. Huang, R.W. Erwin, Phys. Rev. B51 (1995) 5994.
[13] N. Motoyama, H. Eisaki, S. Uchida, Phys. Rev. Lett. 76 (1996) 3212.
[14] H. Suzumura, H. Yasuhara, A. Furusaki, N. Nagaosa, Y. Tokura, Phys. Rev. Lett. 76 (1996) 2579.
[15] W.E. Pickett, Rev. Mod. Phys. 61 (1989) 433.
[16] D.J. Scalapino, Phys. Rep. 250 (1995) 325.
[17] K. Yamaguchi, Y. Takahara, T. Fueno, K. Nasu, J. J. Appl. Phys. 26 (1987) L1362; 26 (1987) L2037; 27 (1987) L509.
[18] T. Soda, Y. Kitagawa, T. Onishi, Y. Takano, Y. Shigeta, H. Nagao, Y. Yoshioka, K. Yamaguchi, Chem. Phys. Lett. 319 (2000) 223.
[19] K. Miyagawa, A. Kawamoto, Y. Nakazawa, K. Kanoda, Phys. Rev. Lett. 75 (1995) 1174.
[20] (a) K. Kanoda, Physica C 282–287 (1997) 290;
(b) K. Kanoda, Hyperfine Interact. 104 (1997) 235.
[21] T. Enoki, J. Yamaura, A. Miyazaki, Bull. Chem. Soc. Jpn. 70 (1997) 2005.
[22] H. Tanaka, A. Kobayashi, T. Saito, K. Kawano, T. Naito, H. Kobayashi, Adv. Mater. 8 (1996) 812.
[23] T. Mori, H. Mori, S. Tanaka, Bull. Chem. Soc. Jpn. 72 (1999) 179.
[24] S. Inagaki, R. Kubo, Int. J. Magnetism 4 (1973) 139.
[25] S. Inagaki, J. Phys. Soc. Jpn. 39 (1975) 596.
[26] H. Suhl, B.T. Matthias, L.R. Walker, Phys. Rev. Lett. 3 (1959) 552.
[27] J. Kondo, Prog. Theoret. Phys. 29 (1963) 1.
[28] K. Yamaji, S. Abe, Physica C (1988) 153.
[29] M.J. Rice, H.Y. Choi, Y.R. Wang, Phys. Rev. B44 (1991) 10414.
[30] Y. Asai, Y. Kawaguchi, Phys. Rev. B46 (1992) 1265.
[31] S. Suzuki, S. Okada, K. Nakao, J. Phys. Soc. Jpn. 69 (2000) 2615.
[32] K. Yamaguchi, S. Hayashi, M. Okumura, M. Nakano, W. Mori, Chem. Phys. Lett. 266 (1994) 372.
[33] H. Nagao, M. Nishino, Y. Yoshioka, K. Yamaguchi, Int. J. Quant. Chem. 65 (1997) 947.
[34] H. Nagao, M. Mitani, M. Nishino, Y. Shigeta, Y. Yoshioka, K. Yamaguchi, Int. J. Quant. Chem. 75 (1999) 549.
[35] H. Nagao, M. Nishino, Y. Shigeta, Y. Yoshioka, K. Yamaguchi, J. Chem. Phys. 113 (2000) 11237.
[36] N. Nagao, Y. Kitagawa, T. Kawakami, T. Yoshimoto, H. Saito, K. Yamaguchi, Int. J. Quant. Chem., in press.
[37] P.W. Anderson, Phys. Rev. 124 (1961) 41.
[38] J. Kondo, Prog. Theor. Phys. 32 (1964) 37.
[39] M. Fujiwara, T. Matsushita, K. Yamaguchi, T. Fueno, Synth. Met. 41–43 (1996) 3267.
[40] M. Fujiwara, S. Takamizawa, W. Mori, K. Yamaguchi, Mol. Cryst. Liq. Cryst. 279 (1996) 1.
[41] K. Yamaguchi, M. Nakano, H. Namimoto, T. Fueno, J. J. Appl. Phys. 27 (1988) L1835; 27 (1989) L479; 28 (1989) L672.
[42] M.A. Ruderman, C. Kittel, Phys. Rev. 96 (1954) 99.
[43] T. Kasuya, Prog. Theoret. Phys. 16 (1956) 45.
[44] K. Yoshida, Phys. Rev. 106 (1957) 893.
[45] N. Nagaosa, P.A. Lee, Phys. Rev. 64 (1990) 2450.
[46] P.W. Anderson, The Theory of Superconductivity in the High-T_c Cuprates, Princeton University Press, Princeton, 1997.
[47] J. Hubbard, Proc. Roy. Soc. (London) A276 (1963) 238.
[48] T. Moriya, Y. Takahashi, K. Ueda, J. Phys. Soc. Jpn. 59 (1990) 2905.
[49] P. Monthoux, D. Pines, Phys. Rev. B47 (1993) 6069.
[50] T. Moriya, K. Ueda, J. Phys. Soc. Jpn. 63 (1994) 1871.
[51] S. Koikegami, S. Fujimoto, K. Yamada, J. Phys. Soc. Jpn. 66 (1997) 1438.
[52] T. Mori, H. Mori, S. Tanaka, Bull. Chem. Soc. Jpn. 71 (1999) 179.
[53] Y. Imamura, S. Ten-no, K. Yonemitsu, Y. Tanimura, J. Chem. Phys. 111 (1999) 5986.
[54] A. Fortunelli, A. Painelli, Phys. Rev. B55 (1997) 16088.
[55] (a) H. Seo, H. Fukuyama, J. Phys. Soc. Jpn. 66 (1997) 3352; (b) H. Seo, H. Fukuyama, J. Phys. Soc. Jpn. 67 (1998) 1848.
[56] H. Kino, H. Fukuyama, J. Phys. Soc. Jpn. 64 (1995) 2726.
[57] H. Kino, H. Kotani, J. Phys. Soc. Jpn. 67 (1998) 3691.
[58] H. Kondo, T. Moriya, J. Phys. Soc. Jpn. 67 (1998) 3695.
[59] T. Judo, S. Koikegami, K. Yamada, J. Phys. Soc. Jpn. 68 (1999) 1331.
[60] S. Murakami, N. Nagaosa, J. Phys. Soc. Jpn. 69 (2000) 2395.
[61] M. Fujiwara, M. Nishino, S. Takamizawa, W. Mori, K. Yamaguchi, Mol. Cryst. Liq. Cryst. 286 (1996) 185.
[62] K. Yamaguchi, M. Okumura, T. Fueno, K. Nakasuji, Synth. Met. 41–43 (1991) 3631.
[63] F. Matsuoka, Y. Yamashita, T. Kawakami, Y. Kitagawa, Y. Yoshioka, K. Yamaguchi, Polyhedron 20 (2001) 1169.
[64] K. Yamaguchi, H. Namimoto, T. Fueno, T. Nogami, Y. Shirota, Chem. Phys. Lett. 166 (1990) 408.
[65] S. Nakasuji, A. Hirai, J. Yamada, K. Suzuki, T. Enoki, H. Anzai, Mol. Cryst. Liq. Cryst. 306 (1997) 409.
[66] H. Sakurai, A. Izuoka, T. Sugawara, Mol. Cryst. Liq. Cryst. 306 (1997) 414.
[67] K. Yamaguchi, Kinozairyo 7 (1990) 5 in Japanese.
[68] T. Mori, H. Inokuchi, Bull. Chem. Soc. Jpn. 61 (1988) 591.
[69] T. Mallah, C. Hollis, S. Bott, M. Kurmoo, P. Day, J. Chem. Soc. Dalton Trans. (1990) 859.
[70] M. Kurmoo, P. Day, P. Guinneau, G. Bravic, D. Chassesu, L. Ducasse, M.L. Allan, I.D. Marsden, R.H. Friend, Inorg. Chem. 35 (1996) 4719.
[71] P. Day, M. Kurmoo, T. Makkah, I.R. Marsden, M.L. Allan, R.H. Friend, F.L. Pratt, W. Hayes, D. Chasseau, G. Bravic, L. Ducasse, J. Am. Chem. Soc. 114 (1992) 10722.
[72] C.J. Gomez-Garcia, L. Ouahab, C.G. -Saiz, S. Triki, E. Koronado, P. Dehaes, Angew. Chem. Int. Ed. Engl. 33 (1994) 323.
[73] J. Yamaura, K. Suzuki, Y. Kaizu, T. Enoki, K. Murata, G. Saito, J. Phys. Soc. Jpn. 65 (1996) 2645.
[74] I.R. Marsden, M.L. Allan, R.H. Friend, M. Kurmoo, D. Kanazawa, P. Day, G. Bravic, D. Chasseau, L. Ducasse, W. Hayes, Phys. Rev. B50 (1994) 2118.
[75] M. Kurmoo, A.W. Graham, P. Day, S.J. Coles, M.B. Hursthouse, J.L. Caulfield, J. Singleton, F.L. Pratt, W. Hayes, L. Ducasse, P. Guionneau, J. Am. Chem. Soc. 117 (1995) 12209.
[76] H. Kobayashi, H. Tomita, T. Naito, A. Kobayashi, F. Sakai, T. Watanabe, P. Cassoux, J. Am. Chem. Soc. 118 (1996) 368.

[77] H. Akutsu, K. Kato, E. Ojima, H. Kobayashi, H. Tanaka, A. Kobayashi, Phys. Rev. B58 (1998) 9294.
[78] L. Brossard, R. Clerac, C. Coulson, M. Tokumoto, T. Ziman, D.K. Petrov, V.N. Laukhin, M.J. Naughton, A. Audouard, F. Goze, A. Kobayashi, H. Kobayshi, P. Cassoux, Eur. J. Phys. B1 (1998) 439.
[79] H. Tanaka, A. Kobayashi, A. Sato, H. Akutsu, H. Kobayashi, J. Am. Chem. Soc. 121 (1999) 760.
[80] A. Sato, E. Ojima, H. Akutsu, Y. Nakazawa, H. Kobayashi, H. Tanaka, A. Kobayashi, P. Cassoux, Phys. Rev. B61 (2000) 111.
[81] H. Kobayashi, A. Kobayashi, P. Cassoux, Chem. Soc. Rev. 29 (2000) 325.
[82] H. Fujiwara, E. Fujiwara, Y. Nakazawa, B.Z. Narymbetov, K. Kato, H. Kobayashi, A. Kobayashi, M. Tokumoto, P. Cassoux, J. Am. Chem. Soc. 123 (2001) 306.
[83] C. Hotta, H. Fukuyama, J. Phys. Soc. Jpn. 69 (2000) 2577.
[84] E. Coronado, J.R. Galan-Mascaros, G.J. Gomez-Garcia, V. Laukhin, Nature 408 (2000) 447.
[85] A. Dei, D. Gatteschi, L. Pardi, U. Russo, Inorg. Chem. 30 (1991) 2589.
[86] S. Kawata, S. Kitagawa, M. Kondo, I. Furuchi, M. Munakata, Angew. Chem. Int. Ed. 33 (1994) 1759.
[87] P.W. Anderson, Science 235 (1987) 1196.
[88] K. Yamaguchi, Y. Takahara, T. Fueno, K. Nakasuji, I. Murata, Jpn. J. Appl. Phys. 27 (1988) 766.
[89] E. Fradkin, Field Theories of Condensed Matter Systems, Addison Wesley, 1991.
[90] K. Awaga, A. Yamaguchi, T. Okuno, T. Inabe, T. Nakamura, M. Matsumoto, Y. Maruyama, J. Mater. Chem. 4 (1994) 1377.
[91] O.M. Yagi, G. Li, H. Li, Nature 378 (1995) 703.
[92] O.M. Yagi, C.E. Davis, G. Li, H. Li, J. Am. Chem. Soc. 119 (1997) 2861.
[93] H. Li, M. Eddaoudi, T.L. Groy, O.M. Yaghi, J. Am. Chem. Soc. 120 (1998) 8571.
[94] S.R. Batten, R. Robson, Angew. Chem. Int. Ed. 37 (1998) 1460.
[95] S. Kitagawa, M. Kondo, Bull. Chem. Soc. Jpn. 71 (1998) 1739.
[96] S. Takamizawa, W. Mori, M. Furihata, S. Takeda, K. Yamaguchi, Inorg. Chim. Acta 283 (1998) 268.
[97] S. Takamizawa, K. Yamaguchi, W. Mori, Inorg. Chim. Commun. 1 (1998) 177.
[98] M. Fujita, Acc. Chem. Rec. 32 (1999) 53.
[99] S.S.Y. Chui, S.M.F. Lo, J.P.H. Charmant, A.G. Orpen, I.D. Williams, Science 283 (1999) 148.
[100] T. Kawakami, S. Takamizawa, Y. Kitagawa, T. Maruta, W. Mori, K. Yamaguchi, Polyhedron 20 (2001) 1197.
[101] M. Mitani, D. Yamaki, Y. Takano, Y. Kitagawa, Y. Yoshioka, K. Yamaguchi, J. Chem. Phys. 113 (2000) 10486.
[102] S. Uji, H. Shinagawa, T. Terashima, T. Yakabe, Y. Terai, M. Tokumoto, A. Kobayashi, H. Tanaka, H. Kobayashi, Nature 410 (2001) 908.
[103] V. Jaccarino, M. Peter, Phys. Rev. Lett. 9 (1962) 290.
[104] H.W. Meul, C. Rossel, M. Decroux, O. Fisher, G. Remenyi, A. Briggs, Phys. Rev. Lett. 53 (1984) 497.
[105] P. Konsin, B. Sorkin, Phys. Rev. B 58 (1998) 5795.